Materials Science and Engineering A 527 (2010) 5287–5294

Contents lists available at ScienceDirect

Materials Science and Engineering A

journal homepage: www.elsevier.com/locate/msea

The influence of cooling rate on the microstructures and mechanical properties in ultrafine-grained aluminum processed by hot rolling

P.L. Sun[a,*], Y.H. Zhao[b], T.Y. Tseng[c], J.R. Su[c], E.J. Lavernia[b]

[a] Department of Materials Science and Engineering, Feng Chia University, Taichung 40724, Taiwan
[b] Department of Chemical Engineering and Materials Science, University of California, Davis, CA 95616, USA
[c] New Materials Research and Development Department, China Steel Corporation, Kaohsiung 81233, Taiwan

ARTICLE INFO

Article history:
Received 17 March 2010
Accepted 27 April 2010

Keywords:
Ultrafine-grained aluminum
Hot and cold rolling
Cooling rate
Microstructures
Mechanical property

ABSTRACT

Commercially pure aluminum AA1050 was processed by hot rolling followed by subsequent water quenching (WQ) and furnace cooling (FC). The samples processed via these two approaches were then cold rolled to obtain ultrafine-grained (UFG) structures. Mechanical behavior studies showed that the WQ UFG Al exhibited a yield stress of 178 MPa and a total elongation of 5.3%, which are higher than those of the FC UFG Al (162 MPa and 3.1%, respectively). Microstructural analyses revealed that the origin of the high strength of the WQ UFG Al is attributable to smaller grain dimensions in the quenched and rolled material. The measured enhanced ductility was rationalized on the basis of three mechanisms: first, improved dislocation accumulation; second, a higher rate of strain hardening due to solid solution pinning during plastic deformation; and third, an increased proportion of high-angle grain boundaries.

1. Introduction

The development of severe plastic deformation (SPD) techniques during the past decade or so has facilitated the production of bulk, ultrafine-grained (UFG) and nanostructured (NS) metals [1–6], which in turn has allowed fundamental study of the mechanical behavior and deformation mechanisms of materials with these length scales. However, bulk UFG/NS materials usually have poor ductility [7–16], low thermal stability [17] and high synthesis cost which are *major concerns* for the technological applications as structural materials. A good ductility is essential for structural components to avoid catastrophic failure in load-bearing applications. Moreover, ductility is also very important for many shaping and forming operations [18]. The low thermal stability of bulk NS materials is caused by their non-equilibrium high-energy state due to their high volume fraction of lattice imperfections (such as dislocations and grain boundaries). High synthesis cost is attributed to the preparation complexity.

Low tensile ductility in UFG/NS materials can be attributed to the onset of a plastic instability (necking) at an early stage of deformation. According to Considère's criterion [19], strain hardening is required in order to delay the initiation of tensile necking. Strain hardening typically results from the interactions of dislocations as they glide and intersect each other. Typically, large grains provide enough space for significant numbers of dislocation intersections during deformation, while in smaller grains, dislocations move and accumulate at opposing boundaries directly and thereby result in minimal hardening [20]. In the case of UFG/NS materials there are two important observations documented in the literature. First, dislocation activity is low within the grain interiors in UFG/NS metals [21,22], and second, a large proportion of the dislocations that do exist are located in the vicinity of, or at grain boundaries [22,23]. Lloyd [23] suggested that dislocations prefer to concentrate at grain boundaries and facilitate recovery, which results in an increasing rate of dynamic recovery that subsequently reduces the strain hardening rate of fine grained Al alloys. In fact, the reported low tensile ductility of UFG/NS materials has emerged as an important barrier that prevents widespread application of UFG/NS metals. Not surprisingly, review of the recent literature reveals the emergence of various strategies that attempt to improve tensile ductility in UFG/NS materials [11,12,14,24–42]. To date, the enhanced tensile ductility in UFG/NS materials has been achieved by the incorporation of bimodal grain sizes [11,26–28], grain boundary engineering [14,29–35], tailoring stacking fault energy [36–39], second-phase precipitation [40–42], reducing processing artifacts [27,43], phase transformation [44] and high deformation strain rates [45]. However, most of the studies can only increase the tensile ductility with a concomitant reduction in strength. It is likely that materials can either be strong or ductile, but rarely both at the same time [46]. Zhao et al. [40–42] have recently demonstrated that it is possible to simultaneously increase the strength and ductility of NS 2024Al and 7075Al alloys by incorporating very small precipitates into

* Corresponding author. Tel.: +886 4 24517250x5345; fax: +886 4 24510014.
E-mail address: plsun@fcu.edu.tw (P.L. Sun).

0921-5093/$ – see front matter © 2010 Elsevier B.V. All rights reserved.
doi:10.1016/j.msea.2010.04.087

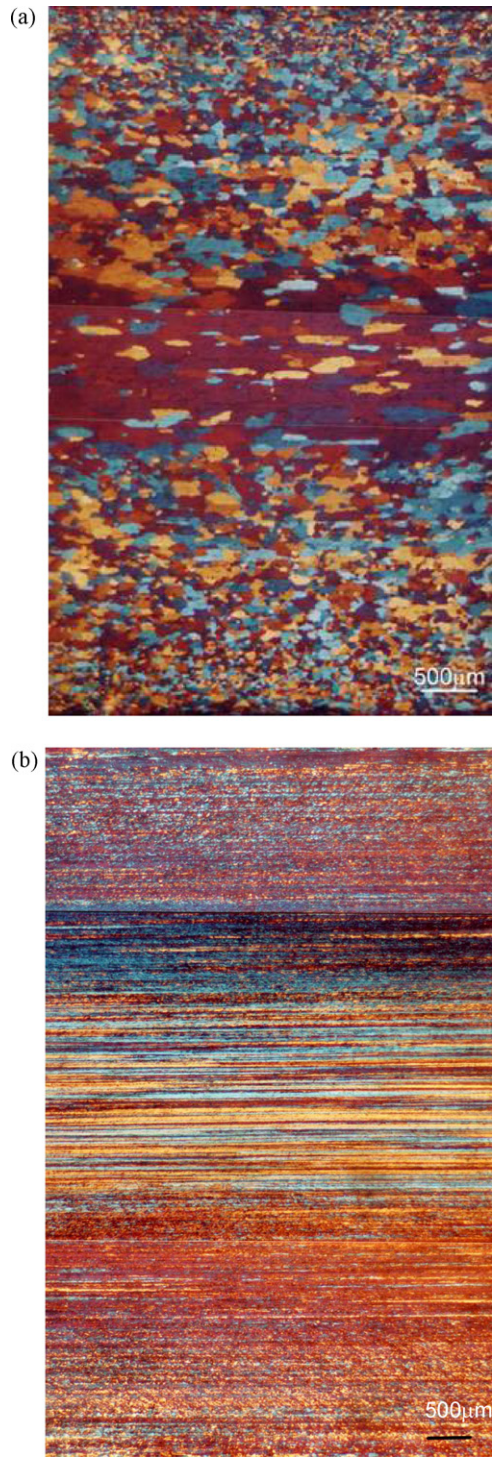

Fig. 1. The optical micrographs of the as-hot rolled (a) FC and (b) WQ specimens.

the NS aluminum matrix. They suggested that the enhancement of strength is due to the presence of second-phase particles, and the enhancement of ductility is due to the increase in strain hardening rate (dislocation accumulation capability) which is further resulted from both dislocation recovery by low-temperature aging and the resistance to dislocation slip by second-phase particles.

The small grains of bulk nanostructured materials can be stabilized by kinetic approaches and thermodynamic strategies [47]. The kinetic stabilization, which involves reduction of the grain boundary mobility, includes second phase drag [48–50], solute drag

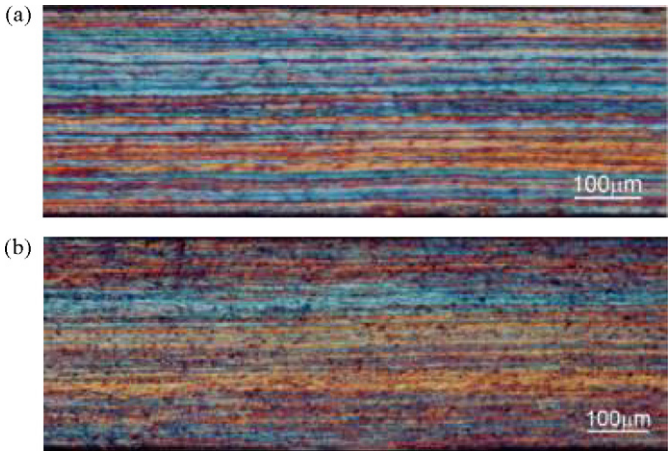

Fig. 2. The optical micrographs of the as-cold rolled (a) FC and (b) WQ specimens.

[51], chemical ordering [52,53], etc., and the thermodynamic stabilization is due to the lowering of the specific grain boundary energy by solute segregation to the grain boundary [54,55]. The two most important SPD techniques are equal-channel angular pressing (ECAP) and high-pressure torsion (HPT) [56]. However, commercialization of bulk NS materials is difficult due to high preparation cost although many efforts have been paid to develop new processing techniques to lower the preparation cost, such as continuous ECAP [57] and accumulative rolling bonding (ARB) [58].

In the present work, three principal strategies are demonstrated. First, it is shown that UFG aluminum can be produced by combination of hot and cold rolling, which is significant from its industrial application potential by lowering the preparation cost. Second, we demonstrated an evident influence of cooling rate following hot rolling on the mechanical properties, i.e. water quenching (WQ) following hot rolling process resulted in both high strength and ductility in comparison with furnace cooling. Finally, we performed systematic microstructural analyses and rationalize that high strength of the WQ UFG Al is attributable to smaller grain dimensions and the enhanced tensile ductility is resulted from the improved dislocation accumulation capability due to solid solution pinning and higher fraction of high-angle grain boundary.

2. Experimental

2.1. Sample preparation

A commercially pure aluminum AA1050 with the chemical composition in wt% of 0.089 Si, 0.216 Fe, 0.001 Cu, 0.02 Ti and balance Al was homogenized at 863 K for 9 h, hot rolled from a thickness of 110 mm to 6 mm and followed with different cooling speeds: furnace cooled (FC) and water quenched (WQ). Hot rolling was performed at a starting temperature of 743 K and final temperature of 643 K. The FC specimen was then kept in the power-off furnace at a temperature of 643 K and slowly cooled to room temperature. These two materials were then cold rolled to a final thickness of 0.3 mm corresponding to a total reduction of ~95%.

2.2. Microstructural analyses

The as-hot rolled and as-cold rolled samples were examined by the use of optical microscope (OM). Grain morphology and grain size of as-rolled transverse planes of the specimens were observed.

Transverse direction (TD) of the as-cold rolled specimens were mechanically thinned down to about 150 μm thickness and final polished with a standard twin-jet polishing method using an electrolyte of 25% nitric acid and 75% methanol at 243 K and 15 V. The

microstructure characterization was conducted in Philips CM200 and FEI Tecnai F20 G2 transmission electron microscopes (TEM) at 200 kV. Three microstructural parameters, grain length, grain width and aspect ratio were determined from the TEM images. Second phase particles were also examined.

Electron backscattering diffraction (EBSD) of the TD plane of the as-cold rolled FC and WQ specimens were obtained by automatic scanning with steps (pixel size) of 80 nm and 50 nm for FC and WQ specimens, respectively. The EBSD mapping was carried out using a field emission gun scanning electron microscope (JSM-6330TF) equipped with a HKL Channel 5 system. Boundary structures of the two samples are analyzed by the use of EBSD.

X-ray diffraction (XRD) measurements of the as-rolled and tensile tested specimens were completed using Cu Kα radiation to estimate the dislocation densities. The θ–2θ scans were conducted at room temperature at a scan speed of 1°/min. Pure aluminum annealed at 673 K was used as an XRD peak-broadening reference for both grain size and microstrain calculations. The peak parameters, including the peak intensity, the integral breadth and the full-width half-maximum, were determined utilizing Microcal (TM) Origin® by fitting a Lorentzian function to the measured peaks. XRD results were averaged from the gauge sections.

2.3. Electrical measurements

The amount of solid solution atoms can be deduced on the basis of electrical conductivity measurements which are reported as a percent of the International Annealed Copper Standard (IACS). The conductivity of the annealed copper is defined to be 100% IACS at 293 K. All other conductivity values are related back to this conductivity of annealed copper. A Nortec-17 model from Staveley Instruments is used for IACS measurements. Standard copper and aluminum specimens were first measured with a probe to calibrate the IACS reading. The FC and WQ specimens were then measured to obtain the IACS values.

2.4. Tensile testing

Uniaxial tensile tests of the as-cold rolled specimens were carried out employing a Sintech 10/GL test machine at an initial strain rate of $1.67 \times 10^{-3}\ s^{-1}$ at ambient temperature. The dimensions of gauge section of the dog bone shaped specimen were 70 mm in length, 25 mm in width and 0.3 mm in thickness. The tensile test axis was parallel to the rolling direction. Duplicate tests were conducted to ascertain reproducibility.

3. Results and discussions

3.1. Microstructures

3.1.1. Grain size and morphology

Macrostructures of the as-hot rolled FC and WQ samples are shown in Fig. 1. The OM images reveal that the as-hot rolled FC and WQ macrostructures are not homogeneous. Grain size increases from the sample surface to the center in both specimens. Moreover, the as-hot rolled FC sample has a much larger grain size than the WQ sample due to recrystallization and grain growth during FC process. The average grain sizes of three areas (surface, sub-surface and center areas) in the FC specimen, measured by linear intercept method, are 30 μm, 50 μm and 70 μm, respectively. The grain sizes in the hot rolled WQ sample are not measured because they are too small and beyond the measurement limit of OM methods.

The as-cold rolled microstructures were characterized by OM, XRD, EBSD and TEM. The macrostructures of the as-cold rolled FC and WQ specimen are shown in Fig. 2. Lamellar rolling structure is evident in both samples. The boundary spacing of the FC specimen

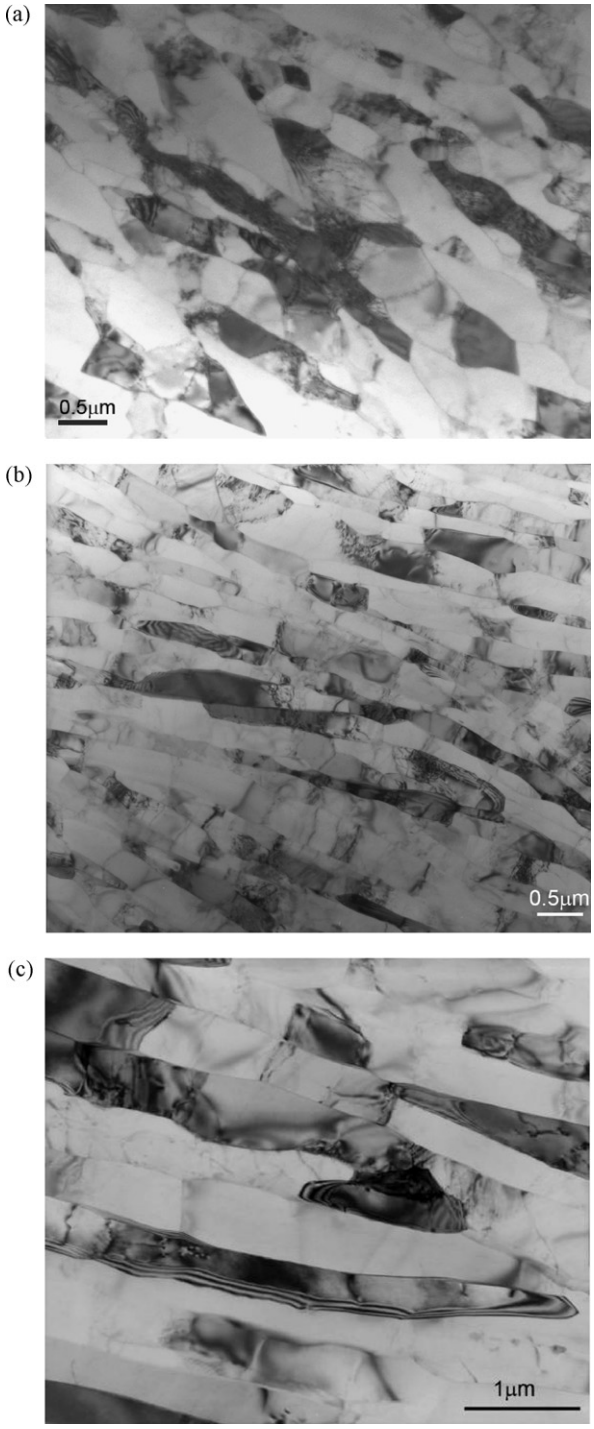

Fig. 3. The as-rolled microstructures of (a) FC specimen, (b and c) WQ specimen. (c) Grains with large aspect ratio and boundary fringe.

is slightly larger than the WQ specimen. Fig. 3 shows the typical TEM microstructures of FC and WQ specimens. Grains are more equiaxed in the FC specimens (Fig. 3a) while they are more elongated in the WQ specimens (Fig. 3b). This could be explained by the macrostructural differences in the hot rolled stage (see Fig. 1) where the FC sample has equiaxed grains due to recrystallization and grain growth. Dislocation densities are high in both samples. The average dislocation density in the FC and WQ specimens, measured by XRD peaking broadening method [59–62], are $2.3 \times 10^{13}\ m^{-2}$ and $2.2 \times 10^{13}\ m^{-2}$, respectively. An extensive examination of the microstructures showed that grain boundary thickness fringes can

Table 1
Microstructure parameters (grain length and width, aspect ratio, fraction of high-angle grain boundary (HAGBs), dislocation density ρ) of the FC and WQ cold rolled specimens.

	Grain length (nm)	Grain width (nm)	Aspect ratio	HAGBs (%)	ρ (m^{-2})
FC	1000	350	2.9	12	2.3×10^{13}
WQ	1000	230	4.4	27	2.2×10^{13}

be more easily observed in the WQ specimens (Fig. 3c). Grain length, grain width and aspect ratio were obtained from the TEM images and summarized in Table 1 and Fig. 4. The average lengths are similar in both samples (1000 nm) while the grain width is about one-third smaller in the WQ specimens (230 nm in WQ vs. 350 nm in FC), which corresponds to a higher aspect ratio (4.4 in WQ vs. 2.9 in FC). The larger grain width in the FC sample was caused by grain growth during furnace cooling. Grain length distributions show that WQ specimens have wider range of grain lengths compared to the FC specimens but the majority grains have a length smaller than 2000 nm (Fig. 4a and b). On the other hand, the grain width range of the FC specimens is larger than that of the WQ specimens (Fig. 4c and d). The grain aspect ratio distribution of the WQ specimens is much wider than in the FC specimens (from 1 to 11), where the majority grains have an aspect ratio between 1 and 5.5 (Fig. 4e and f).

3.1.2. Grain boundary

Boundaries with misorientation angles above 15–20° are defined as high-angle boundaries (HABs) based on energy consider-

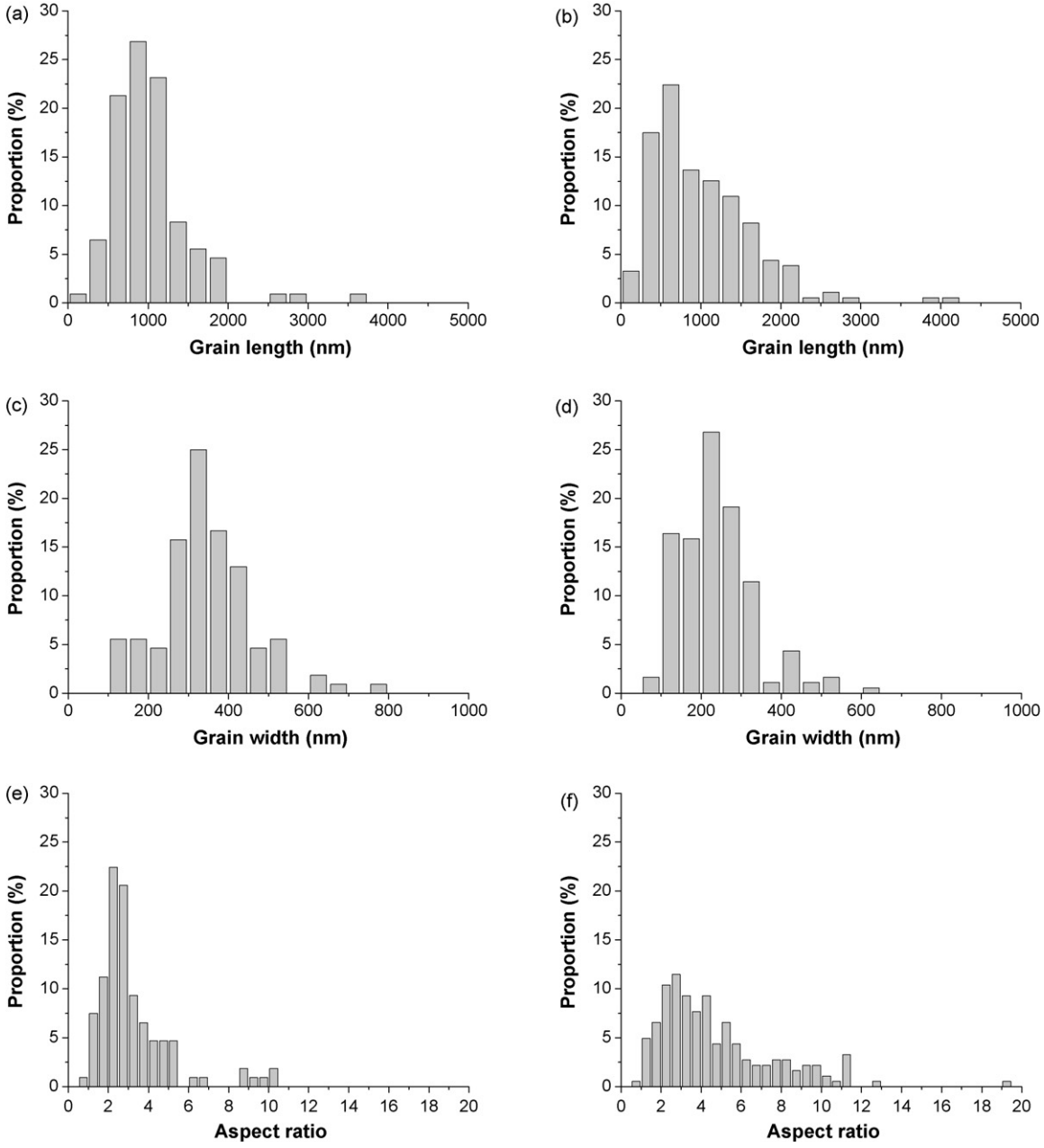

Fig. 4. Grain length distributions of the (a) FC specimen and (b) WQ specimen. Grain width distributions of the (c) FC specimen and (d) WQ specimen. Grain aspect ratio distributions of the (e) FC specimen and (f) WQ specimen.

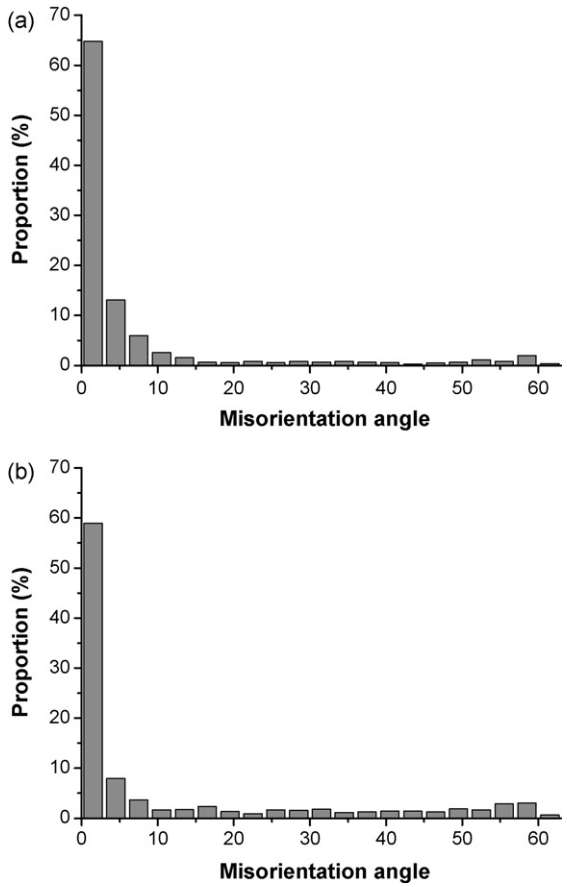

Fig. 5. Grain boundary misorientation distributions of the (a) FC specimen and (b) WQ specimen.

ations [63]. For convenience, HABs are defined as boundaries with misorientation angles greater than 15° whereas low angle boundaries (LABs) have misorientation angles smaller than 15° [64]. Fig. 5 shows the EBSD results. It can be seen that large fractions of the boundaries are LABs in both samples. HABs proportions are 12% and 27% for FC and WQ specimens, respectively. The average misorientation angles above 1° are 7.3° and 12.6° for FC and WQ specimens, respectively. A study by Oscarsson et al. [65,66] shows that when the rolling reduction is greater than 95% in the strip-cast (continuous casting) AA1145, AA1120 and AA8011 aluminum alloys, the majority of the grain boundaries are HABs. It was also experimentally proved that severe plastic deformation can transform LABs to HABs by accumulating dislocations at the boundaries [21]. The total rolling reduction of the present work is 95%. However, the HABs proportions of the two samples are still low compared to Oscarsson's work. This may be attributed to the lower concentration of solution atoms in the present samples compared to their strip-cast alloys. Room temperature is $\sim 0.32T_m$ (homologous temperature) in aluminum, which is higher than other fcc metals (0.17 for nickel and 0.22 for copper); therefore dynamic recovery (dislocation annihilation) can occur at room temperature. With the presence of solid solution atoms, dislocations can be dragged, retained and accumulated at grain boundaries. All of these factors can facilitate HABs formation.

3.1.3. Solid solution and precipitates

Iron and silicon atoms are the main solutes in the commercial purity aluminum and their contents are 0.089 Si, 0.216 Fe wt% in the aluminum matrix, respectively. However, at ambient temperature only small amounts of silicon and iron are soluble in aluminum: 1.65 wt% for silicon and 0.052 wt% for iron. Therefore, the extra 0.164 wt% iron will be trapped at aluminum lattice during WQ and form super-saturated solid solution, which will be transformed into 2nd phase precipitates during FC [67,68].

Our XRD results (as listed in Table 2) indicate that the lattice parameters of the WQ specimens are evidently larger than those of FC specimens. Both hot and cold rolled WQ specimens have comparable lattice parameters (0.40521 nm and 0.40522 nm, respectively), which are larger than those of the hot and cold rolled FC specimens (0.40500 nm and 0.40502 nm, respectively). The coarse-grained (CG) Al reference sample has a lattice parameter of 0.40494 nm, slightly smaller than those of the FC specimens. The large lattice parameters of the WQ specimens verify its super-saturated iron solution. The slightly larger lattice parameters of the FC specimens in comparison of CG Al are because the FC specimens still have some certain small amount of solutes in their lattice. The comparable lattice parameters of the specimens before and after cold rolling indicate that cold rolling did not change the solution atmosphere.

To obtain more detailed results, we performed careful TEM observation, and found that second phase precipitates heterogeneously distribute in the Al matrix of the cold rolled FC specimen, where some areas have slightly higher density of second phase particle (Fig. 6a) but some areas have low density/none of second phase particle (Fig. 6b). These particles are needle-like and globular AlFeSi according to energy dispersive spectroscopy (EDS) and selected area electron diffraction (SAED) analysis. The long axis and short axis of needle-like AlFeSi are ranging from 90 to 277 nm and 40 to 110 nm, respectively. The globular AlFeSi are smaller than the needle-like particles and have the size of 40–120 nm. The average spacing between these second-phase particles is calculated to be $\sim$1 μm. However, the real average spacing is larger than this value because this value is only averaged from areas with the presence of second phase particles. Careful TEM observation did show some second-phase particles in the cold rolled WQ specimen. However, the precipitate density is very low and the average spacing between them is 40 μm. Therefore, the influence of the second-phase particles in the WQ specimen can be neglected. XRD measurement did not reveal the presence of second phase particle in both as-cold rolled FC and WQ specimens due to the very small amount of the particles. The above TEM results indicate that the super-saturated solid solute of iron was transformed into AlFeSi precipitate during FC process, in good agreement with the XRD results. Regardless of the small difference in iron content in aluminum lattice (0.164 wt%), large influence on mechanical behavior and microstructural evolutions occur due to the large difference in atomic diameters between aluminum and iron, as revealed in the following sections.

3.2. Electrical properties

The electrical conductivities of the as-hot rolled FC and WQ specimens are measured to be 61.2% and 60.6% IACS, respectively. The IACS value of 99.999% pure aluminum was measured as well to provide a direct comparison with the two samples. It is 64% IACS. Higher IACS value indicates better conductivity of electrons. The cold rolled WQ specimen has more solid solution atoms, higher fraction of high-angle grain boundaries, and higher volume fraction of total grain boundaries (due to its small grain width), which impede electron transport and, therefore, lower the IACS value, consistent with the present results.

3.3. Tensile behavior

The tensile engineering stress–strain curves of the FC and WQ specimens are shown in Fig. 7. 99.99% pure aluminum subjected to 98% cold rolling reduction [69] is also included in Fig. 7 for

Table 2
Lattice parameters of the FC and WQ hot rolled and cold rolled specimens as well as coarse-grained Al reference sample.

Samples	WQ		FC		CG Al
	Hot rolled	Cold rolled	Hot rolled	Cold rolled	
Lattice parameters (nm)	0.40521	0.40522	0.40500	0.40502	0.40494

comparison. It can be seen that the WQ specimen has higher 0.2% offset yield stress (YS = 178 ± 1.7 MPa), ultimate tensile stress (UTS = 201 ± 0.7 MPa), elongation to failure (5.3 ± 0.04%) than the 99.99% pure aluminum and FC specimen, which has a YS of 162 ± 2.4 MPa, UTS of 183 ± 0.3 MPa and elongation to failure of 3.1 ± 0.13%. The WQ specimen has smaller boundary spacing than the FC specimen, which is related to its higher stress. The yield stress difference between the WQ and FC specimens is ~16 MPa. According to Hall–Petch relationship in pure aluminum, the grain size difference between the FC and WQ specimens contributes to a yield stress difference of 16 MPa [70,71], consistent with the present study. The presence of second phase particles can also cause precipitation hardening [72]. The average particle spacing of the FC specimen is ~1 μm and contributes to a strength of ~8 MPa according to Orowan equation [72]. However, the real contribution of precipitation hardening is smaller than 8 MPa due to the heterogeneous distribution of the precipitations. On the other hand, the higher solid solution content in the WQ specimen can cause solution hardening. The effect of solution hardening on YS in the WQ specimen is at the same order as the precipitation hardening in the FC specimen due to their yield stress difference is mainly from grain size strengthening.

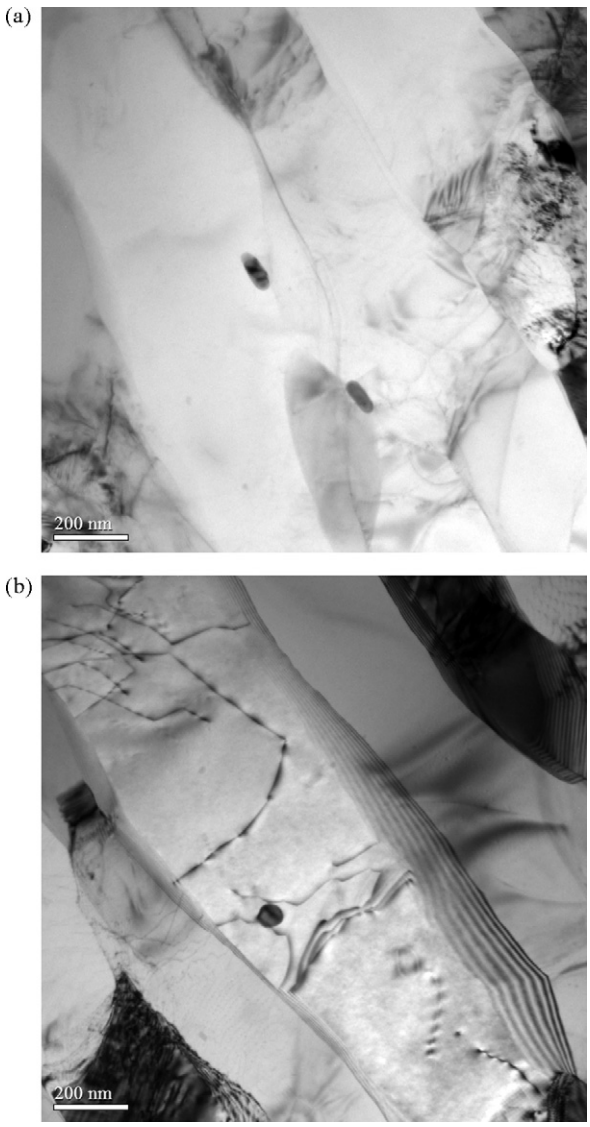

Fig. 6. Higher magnification TEM images show the presence of (a) needle-like and (b) globular AlFeSi second phase particles in the cold rolled FC specimen.

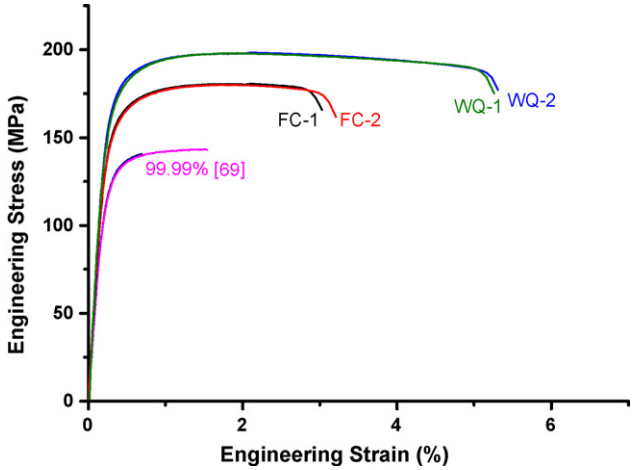

Fig. 7. Engineering stress–strain curves for the FC, WQ commercially pure Al and 99.99% Al specimens.

WQ specimen also exhibits a slightly higher normalized strain hardening rate (Θ), which extends to higher strain than the FC specimen (Fig. 8), is the reason for higher tensile elongation in this UFG aluminum. Θ is defined as $\Theta = 1/\sigma(\partial\sigma/\partial\varepsilon)_{\varepsilon}$, where σ is true stress and ε is true strain. The mechanism responsible for the higher strain hardening rate in the WQ specimen was investigated by XRD analyses of the specimens before and after tensile tests. The dislocation densities of the tensile tested FC and WQ

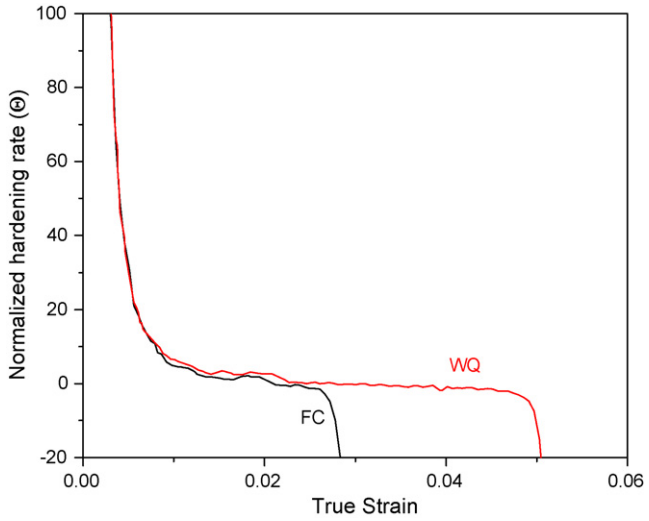

Fig. 8. The normalized strain hardening rate versus true strain for the FC and WQ specimens.

specimen are measured as 2.0×10^{13} m^{-2} to 3.3×10^{13} m^{-2}, respectively. Comparing with the dislocation densities of the untested specimens, the dislocation density increased in the WQ specimen during tensile testing while dislocation density remains similar in the FC specimen ($\sim 2 \times 10^{13}$ m^{-2}). The increase is by ~50% from 2.2×10^{13} m^{-2} to 3.3×10^{13} m^{-2} in the WQ specimen. The solid solution atoms play roles similar to the small second phase particles in the work of Zhao et al. [40–42]. With the presence of solid solution atoms, dislocations can be dragged during plastic deformation, which can significantly hinder dynamic recovery and increase the dislocation storage capability. The work hardening rate is therefore increased. The solid solution atoms also impede dislocation slip, which increases the strength [40–42]. Dislocation densities of the FC specimen are similar before and after tensile test, which indicates that the annihilation of dislocations (dynamic recovery) and creation of dislocations (work hardening) are similar in this sample. It is clear here that without solid solution atoms, dislocation annihilation is more pronounced, and dynamic recovery is more likely to happen. The contents difference of solid solution atoms is very small (<0.2 wt%) in the FC and WQ specimens. However, the small difference in solid solution contents can significantly influence material microstructural and mechanical behavior. The solid solution effect on enhancing tensile ductility and stabilizing necking instability was also observed in Al–Zn solid solution alloy [73]. In addition, it was reported that high fraction of HAGBs could also increase the strain hardening rate and therefore the tensile ductility [36]. The second precipitates in the FC specimens might have very weak effect on the strain hardening and tensile ductility due to its small amount, although in the literature, it was verified that the precipitates could stabilize necking instability [40–42].

To ascertain the solid solution effect, 99.99% pure aluminum subjected to 98% cold rolling reduction [69] is included in Fig. 7. The 99.99% pure aluminum exhibits inferior strength and ductility than both the FC and WQ specimens. WQ specimen has higher solid solution content, and higher YS, UTS and tensile elongation can be obtained. However, the elongation to failure is still low in the two specimens. The tensile elongation (especially post-necking part) depends on the gauge length of the tested specimen and strain measurement method [74,75]. Long gauge length (70 mm) is used in the present work and the elongation is therefore small.

It should be noted that XRD analysis only provides qualitative estimates of the dislocation densities but not a direct measure of the absolute values. For instance, XRD and TEM analyses may yield values for the dislocation densities that vary by an order of magnitude in similar specimens [36,76]. Nevertheless, it is well established that relative dislocation densities can be compared in different materials if they are measured and calculated using the same experimental method. Therefore, the relative change of dislocation density before and after tensile tests corresponds to a valid trend for these two specimens.

4. Summary

This work demonstrates two principal strategies. First, it is shown that UFG aluminum can be produced by rolling, which is significant from its industrial application potential by lowering the fabrication costs. Second, this paper investigates the effect of small solid solution content on the microstructures and mechanical behavior of a commercially pure UFG aluminum.It is shown that higher solid solution content leads to smaller grain width after rolling. Additionally, higher solid solution content in UFG Al can simultaneously increase the tensile strength and ductility. The higher tensile strength is facilitated by the smaller grain width after rolling. The improved ductility in tensile test is attributed to the improved dislocation accumulation and higher rate of strain hardening results from solid solution pinning effect during plastic deformation.This strategy can be adapted to the commercial aluminum alloys to obtain both high strength and ductility in combination. High cooling speed after hot rolling or higher homogenization temperature can be easily performed in the industry, which can retain high solid solution atoms and facilitate favorable tensile behavior.

Acknowledgements

This work was supported by the National Science Council of ROC under contract NSC-96-2218-E-035-008 and NSC-97-2221-E-035-012. Y.H. Zhao and E.J. Lavernia would like to acknowledge support by the Office of Naval Research (Grant number N00014-08-1-0405) with Dr. Lawrence Kabacoff as program officer.

References

[1] M. Richert, Q. Liu, N. Hansen, Mater. Sci. Eng. A260 (1999) 275–283.
[2] Y. Saito, H. Utsunomiya, N. Tsuji, T. Sakai, Acta Mater. 47 (1999) 579–583.
[3] V.M. Segal, Mater. Sci. Eng. A197 (1995) 157–164.
[4] I. Saunders, J. Nutting, Metal Sci. 18 (1984) 571–575.
[5] P.L. Sun, P.W. Kao, C.P. Chang, Mater. Sci. Eng. A283 (2000) 82–85.
[6] P.L. Sun, P.W. Kao, C.P. Chang, Metall. Mater. Trans. 35A (2004) 1359–1368.
[7] C.C. Koch, D.G. Morris, K. Lu, A. Inoue, MRS Bull. 24 (1999) 54–58.
[8] C.C. Koch, Scr. Mater. 49 (2003) 657–662.
[9] E. Ma, Scr. Mater. 49 (2003) 663–668.
[10] S. Cheng, J.A. Spencer, W.W. Milligan, Acta Mater. 51 (2003) 4505–4518.
[11] Y. Wang, M.W. Chen, F.H. Zhou, E. Ma, Nature 419 (2002) 912–915.
[12] Y. Wang, E. Ma, Acta Mater. 52 (2004) 1699–1709.
[13] C.Y. Yu, P.L. Sun, P.W. Kao, C.P. Chang, Scr. Mater. 52 (2005) 359–363.
[14] P.L. Sun, C.Y. Yu, P.W. Kao, C.P. Chang, Scr. Mater. 52 (2005) 265–269.
[15] P.C. Hung, P.L. Sun, C.Y. Yu, P.W. Kao, C.P. Chang, Scr. Mater. 53 (2005) 647–652.
[16] Y.H. Zhao, Y. Li, T.D. Topping, X.Z. Liao, Y.T. Zhu, R.Z. Valiev, E.J. Lavernia, Int. J. Mater. Res. 100 (2009) 1647–1652.
[17] K. Zhang, J.R. Weertman, J.A. Eastman, Appl. Phys. Lett. 87 (2005) 061921.
[18] B. Dodd, Y. Bai, Ductility Fracture and Ductility—With Applications to Metalworking, Harcourt Brace Javanovich, Academic Press Inc., London, UK, 1987.
[19] G.E. Dieter, Mechanical Metallurgy, 3rd ed., McGraw-Hill Book Co., New York, NY, 1988, pp. 289–290.
[20] G.E. Dieter, Mechanical Metallurgy, 3rd ed., McGraw-Hill Book Co., New York, NY, 1986, pp. 231–233.
[21] C.P. Chang, P.L. Sun, P.W. Kao, Acta Mater. 48 (2000) 3377–3385.
[22] P.L. Sun, E.K. Cerreta, G.T. Gray III, J.F. Bingert, Metall. Mater. Trans. 37A (2006) 2983–2994.
[23] D.J. Lloyd, Metal Sci. 14 (1980) 193–198.
[24] Y.H. Zhao, Y.T. Zhu, E.J. Lavernia, Adv. Eng. Mater., in press.
[25] Y.H. Zhao, X.Z. Liao, Mater. Sci. Forum. 633–634 (2010), 3-0.
[26] V.L. Tellkamp, A. Melmed, E.J. Lavernia, Metall. Mater. Trans. A 32 (2001) 2335–2343.
[27] Y.H. Zhao, T. Topping, J.F. Bingert, A.M. Dangelewicz, Y. Li, W. Liu, Y.T. Zhu, Y.Z. Zhou, E.J. Lavernia, Adv. Mater. 20 (2008) 3028–3033.
[28] O. Ertorer, T.D. Topping, Y. Li, Y.H. Zhao, W. Moss, E.J. Lavernia, Mater. Sci. Forum 633–634 (2010) 459–469.
[29] L. Lu, L.B. Wang, B.Z. Ding, K. Lu, J. Mater. Res. 14 (2000) 270–273.
[30] P.L. Sun, E.K. Cerreta, G.T. Gray III, P. Rae, Mater. Sci. Eng. A410–411 (2005) 265–268.
[31] P.L. Sun, E.K. Cerreta, J.F. Bingert, G.T. Gray III, M.F. Hundley, Mater. Sci. Eng. A464 (2007) 343–350.
[32] R.Z. Valiev, I.V. Alexandrov, Y.T. Zhu, C.T. Lowe, J. Mater. Res. 17 (2002) 5–8.
[33] R.K. Islamgaliev, N.F. Yunusova, I.N. Sabirov, A.V. Sergueeva, R.Z. Valiev, Mater. Sci. Eng. A319–321 (2001) 877–881.
[34] Y.H. Zhao, J.F. Bingert, Y.T. Zhu, X.Z. Liao, R.Z. Valiev, Z. Horita, T.G. Langdon, Y.Z. Zhou, E.J. Lavernia, Appl. Phys. Lett. 92 (2008) 081903.
[35] Y.H. Zhao, J.F. Bingert, X.Z. Liao, B.Z. Cui, K. Han, A. Serhueeva, A.K. Muhkerjee, R.Z. Valiev, T.G. Langdon, Y.T. Zhu, Adv. Mater. 18 (2006) 2949–2953.
[36] Y.H. Zhao, Y.T. Zhu, X.Z. Liao, Z. Horita, T.G. Langdon, Appl. Phys. Lett. 89 (2006) 121906.
[37] Y.H. Zhao, X.Z. Liao, Z. Horita, T.G. Langdon, Y.T. Zhu, Mater. Sci. Eng. A493 (2008) 123–129.
[38] P.L. Sun, Y.H. Zhao, J.C. Cooley, M.E. Kassner, Z. Horita, T.G. Langdon, E.J. Lavernia, Y.T. Zhu, Mater. Sci. Eng. A 525 (2009) 83–86.
[39] E. Chew, H.H. Kim, C. Ferraris, Y.H. Zhao, E.J. Lavernia, C.C. Wong, Mater. Sci. Forum 633–634 (2010) 449–457.
[40] Y.H. Zhao, X.Z. Liao, S. Cheng, E. Ma, Y.T. Zhu, Adv. Mater. 18 (2006) 2280–2283.
[41] S. Cheng, Y.H. Zhao, Y.T. Zhu, E. Ma, Acta Mater. 55 (2007) 5822–5832.
[42] Y.H. Zhao, X.Z. Liao, Z. Jin, R.Z. Valiev, Y.T. Zhu, Acta Mater. 52 (2004) 4589–4599.
[43] Y.H. Zhao, Q. Zhan, T.D. Troy, Y. Li, W. Liu, E.J. Lavernia, Mater. Sci. Eng. A527 (2010) 1744–1750.

[44] S. Cheng, H. Choo, Y.H. Zhao, X.L. Wang, Y.T. Zhu, Y.D. Wang, J. Almer, P.K. Liao, J.E. Jin, Y.K. Lee, J. Mater. Res. 23 (2008) 1578–1586.
[45] S. Cheng, Y.H. Zhao, Y. Guo, Y. Li, Q. Wei, X.-L. Wang, Y. Ren, P.K. Liaw, H. Choo, E.J. Lavernia, Adv. Mater. 21 (2009) 5001–5004.
[46] R.Z. Valiev, Nature 419 (2002) 887–889.
[47] C.C. Koch, R.O. Scattergood, K.A. Darling, J.E. Semones, J. Mater. Sci. 43 (2008) 7264–7272.
[48] F.J. Humphreys, M. Hatherly, Recrystallization and Related Annealing Phenomena, Elsevier Science Inc., Tarrytown, NY, 1996, p. 281 (Chapter 9).
[49] R.J. Perez, H.G. Jiang, C.P. Dogan, E.J. Lavernia, Metall. Mater. Trans. A 29 (1998) 2469–2475.
[50] L. Shaw, H. Luo, J. Villegas, D. Miracle, Acta Mater. 51 (2003) 2647–2663.
[51] P. Knauth, A. Charai, P. Gas, Scr. Metall. Mater. 28 (1993) 325–330.
[52] Z. Gao, B. Fultz, Nanostruct. Mater. 2 (1993) 231–240.
[53] C. Bansal, Z. Gao, B. Fultz, Nanostruct. Mater. 5 (1995) 327–336.
[54] B. Farber, E. Cadel, A. Menand, G. Schmitz, R. Kirchheim, Acta Mater. 48 (2000) 789–796.
[55] K.W. Liu, F. Mucklich, Acta Mater. 49 (2001) 395–403.
[56] R.Z. Valiev, R.K. Islamgaliev, I.V. Alexandrov, Prog. Mater. Sci. 45 (2000) 103–189.
[57] J.C. Lee, H.K. Seok, J.H. Han, Y.H. Chung, Mater. Res. Bull. 36 (2001) 997–1004.
[58] X. Huang, N. Hansen, N. Tsuji, Science 312 (2006) 249–251.
[59] L.H. Qian, S.C. Wang, Y.H. Zhao, K. Lu, Acta Mater. 50 (2002) 3425.
[60] Y.H. Zhao, K. Lu, K. Zhang, Phys. Rev. B 66 (2002) 085404.
[61] Y.H. Zhao, K. Zhang, K. Lu, Phys. Rev. B 56 (1997) 14322–14329.
[62] Y.H. Zhao, H.W. Sheng, K. Lu, Acta Mater. 49 (2001) 365–375.
[63] W.T. Read, W. Shockley, Phys. Rev. 78 (1950) 275–289.
[64] D.A. Hughes, N. Hansen, Acta Mater. 45 (1997) 3871–3886.
[65] A. Oscarsson, H.-E. Ekström, B. Hutchinson, Mater. Sci. Forum 113–115 (1993) 177–182.
[66] A. Oscarsson, B. Hutchinson, B. Nicol, P. Bate, H.-E. Ekström, Mater. Sci. Forum 157–162 (1994) 1271–1276.
[67] C.M. Allen, K.A.Q. O'Reilly, B. Cantor, P.V. Evans, Prog. Mater. Sci. 43 (1998) 89–170.
[68] I.S. Lee, P.W. Kao, N.J. Ho, Intermetallics 16 (2008) 1104–1108.
[69] J.H. Chen, M.S. Thesis, National Sun Yat-Sen University, 2007.
[70] N. Hansen, Mater. Sci. Eng. A 409 (2005) 39–45.
[71] N. Kamikawa, X. Huang, N. Tsuji, N. Hansen, Acta Mater. 57 (2009) 4198–4208.
[72] D.K. Felbeck, A.G. Atkins, Strength and Fracture of Engineering Solids, 2nd ed., Prentice Hall Inc., New Jersey, 1996.
[73] C.M. Hu, C.M. Lai, P.W. Kao, N.J. Ho, J.C. Huang, Scr. Mater. 60 (2009) 639–642.
[74] Y.H. Zhao, Y.Z. Guo, Q. Wei, A.M. Dangelewicz, C. Xu, Y.T. Zhu, T.G. Langdon, Y.Z. Zhou, E.J. Lavernia, Scr. Mater. 59 (2008) 627–630.
[75] Y.H. Zhao, Y.Z. Guo, Q. Wei, T.D. Topping, A.M. Dangelewicz, Y.T. Zhu, T.G. Langdon, E.J. Lavernia, Mater. Sci. Eng. A 525 (2009) 68–77.
[76] L. Balogh, T. Ungár, Y.H. Zhao, Y.T. Zhu, Z. Horita, C. Xu, T.G. Langdon, Acta Mater. 56 (2008) 809–820.